Cent. Eur. J. Chem. • 10(6) • 2012 • 1799-1807
DOI: 10.2478/s11532-012-0098-y

VERSITA

Central European Journal of **Chemistry**

The influence of the chelating/combustion agents on the structure and magnetic properties of zinc ferrite

Research Article

Tamara Slatineanu[1], Eliano Diana[2], Valentin Nica[3],Victor Oancea[1], Ovidiu F. Caltun[3], Alexandra R. Iordan[1], Mircea N. Palamaru[1*]

[1]*Faculty of Chemistry, Alexandru Ioan Cuza University of Iasi, Iasi 700506, Romania*

[2]*Department of Chemistry I.F.M., University of Turin, Turin 10125, Italy*

[3]*Faculty of Physics, Alexandru Ioan Cuza University of Iasi, Iasi 700506, Romania*

Received 28 March 2012; Accepted 16 July 2012

Abstract: The present study is reporting the influence of the chelating/combustion agents on the magnetic properties of Zn ferrite. Six chelating/combustion agents, citric acid, egg white, tartaric acid, glycine, glucose and urea, were used to obtain monophase zinc nanoferrite via a sol-gel auto-combustion method. The samples were subjected to a comparative study of structural features and magnetic properties by means of infrared spectroscopy, X-ray diffractometry, scanning electron microscopy and vibrating sample magnetometry. Significant influence of fuel and combustion mode was observed in the magnetic behavior of as-obtained samples. Values of the structural parameters were discovered to vary as a function of fuel choice, and to obtain crystallite size between 38 and 62 nm, inversion degree between 0.239 and 0.807, lattice parameter between 8.4125 and 8.4432 Å. The optimization of sol-gel method synthesis of zinc ferrite nanoparticles by chosing the appropriate fuel is providing structural and magnetic properties of zinc nanoferrite as potential materials to be used in biomedical applications.

Keywords: *$ZnFe_2O_4$ ferrite • Sol-gel • Cation distribution • X-ray diffraction • Magnetic measurements*

1. Introduction

Zinc ferrite has been known for a long time as an oxidic compound with versatile properties, and which can be used as an alternative material in areas devoted to magnetic materials for hyperthermia [1], contrast agents [2], gas sensors [3], catalysts [4], *etc*. During the last decades, many synthesis methods to obtain pure Zn ferrite nanoparticles were developed. High purity and crystallinity were achieved through methods such as as solid state [5,6], coprecipitation [4], hydrothermal [7], microemulsion [2], sol-gel [8,9], thermal decomposition [10], sonolysis [11]. Sol-gel method and its variants, including sol-gel auto-combustion, offer well-known advantages of liquid phase reactions with respect to solid phase reactions. The dispersion of reactants takes place optimally, producing a homogeneous mixture and increasing the reactivity of precursors. Therefore the initiated chemical processes in liquid medium do not require large activation energies. In such processes, the reaction initiation temperature is lower, and the distribution of the as-formed oxide components in the crystalline structure is uniform because of the precursor mixture homogeneity. The importance of fuel choice for auto-combustion process has been investigated in connection with the structural characteristics and physical properties of Zn ferrite nanoparticles. Upadhyay and others [12] prepared zinc ferrite particles of 6 nm using citric acid as fuel and they reported an inversion degree value of 0.40 using a model calculation of $ZnFe_2O_4$ system Columbic energy. Mozaffari and others [13] studied the effect of cation distribution on

* *E-mail: palamaru@uaic.ro*

Table 1. Details of protocol synthesis until annealing stages in the oven.

Sample name	Fuel agent	Molar ratio ferrite: fuel agent	Time of gel formation at 353K	Sand bath temperature at the ignition point	Post-ignition duration until 623K
ZFCA	Citric acid	1:3	2 h	523 K	3 h
ZFEW	Egg white	*	2 h 30 min	523 K	3 h
ZFTA	Tartaric acid	1:3	2 h	573 K	2 h
ZFGLy	Glycine	1:1.5	10 h	423 K	5 h
ZFGLu	Glucose	1:3	2 h	623 K	1 h
ZFU	Urea	1:6	5 h	473 K	4 h

** weight ratio of ferrite:egg white = 1:22.2*

zinc ferrite magnetization at room temperature using sol-gel method and two different fuels citric acid and urea, respectively. At 773 K calcination temperature, they obtained nanoparticles of 13 and 16 nm, respectively. The sample obtained using urea presented nonlinear magnetization at room temperature with very thin hysteresis loops, while the sample obtained using citric acid showed paramagnetic–superparamagnetic type behavior. It was suggested without giving any specific value that the degree of inversion is the cause of this different behavior between the two samples. Hu and others [14] used citric acid for synthesis of zinc ferrite nanoparticles with 35.9 nm after the calcination at 923 K, and they reported paramagnetism at room temperature. The magnetic behavior was explained based on cation distribution and particle size effect without any given inversion degree values.

To our best knowledge, only one study have was conducted recently in the case of Zn ferrite obtained by sol-gel auto-combustion method using natural source of organic matter as fuel agent like aloe vera extract [15].

The present study shows a new comparative approach concerning the obtained values for the inversion degree, crystallite size, lattice parameter, vibrational modes and the specific magnetization registered at room temperature for zinc ferrite samples synthesized using six different chelating/combustion agents citric acid, egg white, tartaric acid, glycine, glucose and urea *via* sol-gel auto-combustion method.

Based on the fact that in the sol-gel synthesis fuel agent is influencing particle size, and thus properties tuning, we have chosen fuel agents from different organic compound classes.

This study reports for the first time, the synthesis of Zn nanoferrite by sol-gel auto-combustion method using egg white and glucose as fuels.

2. Experimental procedure

Nanoparticles of $ZnFe_2O_4$ (ZF) were obtained by sol-gel auto-combustion method using stoichiometric proportions of metal nitrates as cation sources and six different chelating-combustion agents. All the reagents were of analytical purity and were used without additional purification. The appropriate quantities of chelating-combustion agents were used in order to avoid segregation phenomenon and to obtain nanoscale crystallite size: citric acid ($C_6H_8O_7 \cdot H_2O$, Merck), egg white, tartaric acid ($C_4H_6O_6$, Merck), glycine ($C_2H_5NO_2$, Merck), D-(+)-glucose ($C_6H_{12}O_6$, Aldrich) and urea (CH_4ON_2, Merck). Table 1 shows quantitative details of protocol synthesis. A different amount of fuel agent was used due to some previous case studies as examples of the best practice in order to achieve pure spinel phase at the lowest level of thermal treatment [1,8,9,16-18]. Thus, a time range for gel formation is different from time used in other studies, as we proposed to obtain an appropriate consistency of the chemical mixture.

The next step was to dry the gels *via* the sand bath following a step of 50°C h^{-1} starting with the auto-ignition moment. Dried gels were grinded thoroughly to avoid incomplete heat diffusion. In order to complete the spinel phase formation after the sand bath thermal treatment until 623 K, all the samples were heat treated in the oven in normal atmosphere for three separate stages: 7 hours at 773 K, 7 hours at 973 K and 10 hours at 1173 K. Samples were named ZFCA, ZFEW, ZFTA, ZFGLy, ZFGLu, ZFU according to the as-used fuel agents. The initiation and formation of spinel-type phase of ZF samples were monitored by means of spectroscopy in the mid infrared range (KBr pellets technique) using a Bruker VERTEX 70 FT-IR Spectrometer. X-ray diffraction (XRD) patterns of the powders heat treated at 973 K and 1173 K were recorded using a Shimadzu

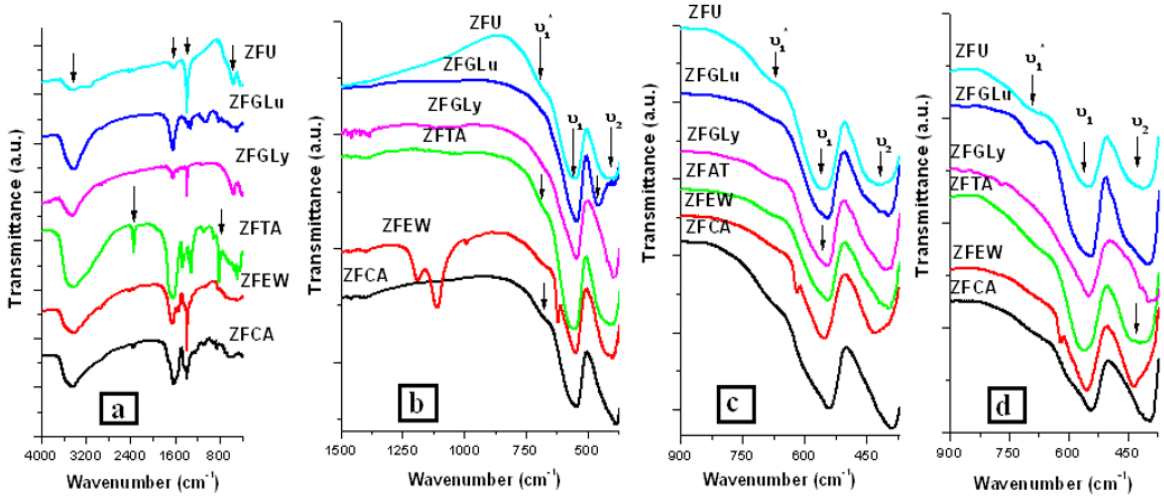

Figure 1. FT-IR data for ZF samples: (a) after heat treatment at 473 K, (b) after heat treatment at 773 K, (c) after heat treatment at 973 K, (d) after heat treatment at 1173 K.

LabX 6000 diffractometer equipped with graphite monochromator and CuK_{α} (λ=0.15406 nm) radiation. The specimens mounted in the reflection mode were analyzed in the ambient atmosphere with a scanning rate of 0.02° and a step of 1° min^{-1} over the 2θ = 20–80° range. The lattice parameter values were calculated using multiple linear regression method based on least-squares procedure, corrected using standard Si powder. X-ray density, physical density and porosity values were calculated for the pure samples after heat treatment at 1173 K according to a similar study [16]. Semi-quantitative analysis of secondary phases was performed according to the method described by Klug and Alexander [19]. An original program was run in order to obtain the inversion degree value of each sample using the appropriate mathematical equations [20], NetBeans IDE integrated development environment and Java programming language. A Vega Tescan-type Scanning Transmission Electron Microscope (SEM) was used to study the morphology, microstructure and macroporosity of ZF samples sintered at 1173 K. In order to determine the influence of the chelating agents and combustion process on the magnetic properties at room temperature of the annealed samples, a Vibrating Sample Magnetometer System (VSM 300 Princeton) was used.

3. Results and discussion

3.1. IR spectra interpretation

IR spectra for ZF dried gels at 473 K (Fig. 1a) indicate the specific absorption peaks of hydroxyl, carboxyl and nitrate ions in the range of 3500-800 cm^{-1}. Broad bands around 3400 cm^{-1} and narrow bands around 1630 cm^{-1}, represent an effect of stretching vibrations of O-H bond interaction via hydrogen bonds. Absorption bands recorded around 1380 cm^{-1} are appropriate stretching vibration of C = O bond of carboxyl ions from byproducts of the combustion agents. The existence of nitrate ions in the precursor gel is indicated by the specific bands appearing in the range of 1090-800 cm^{-1}. The absorption peaks observed below 800 cm^{-1} occur due to M-O (M-metallic cation, O-oxygen anion) bonds vibration where M could be Zn or Fe cations.

A different behavior of the obtained ZF nanopowders depending on employed fuels, post-ignition thermal treatment duration and annealing temperature is evident. Only for ZFGLy and ZFU samples, for which the combustion process was the most spontaneous and violent among the other fuels, the FT-IR data, after the heat treatment at 473 K, show a clear formation of the ZF phase (Fig. 1a).

Vibrational spectra of normal spinel ferrites have four infrared active modes in the crystalline state, according to selection rules for the O_h^7 space group [21]. All the modes are triple degenerated t_{1u} modes, and usually are numbered v_1, v_2, v_3, v_4.

Vibrational modes v_1 and v_2 are assigned, respectively, to tetrahedral and octahedral coordinate ions, and their character is mainly M-O stretching. Literature data report differing frequency values for these modes in the range of 568-536 cm^{-1} for v_1 and of 425-369 cm^{-1} for v_2 [11,21]. Presence of a shoulder close to v_1 and denoted v_1^* could be indicative of the cation

Table 2. FT-IR data for ZF samples heat treated at 773 K, 973 K and 1173 K.

Sample	Vibrational modes after heat treatment at 773 K (cm^{-1})			Vibrational modes after heat treatment at 973 K (cm^{-1})			Vibrational modes after heat treatment at 1173 K (cm^{-1})		
	v_1^*	v_1	v_2	v_1^*	v_1	v_2	v_1^*	v_1	v_2
ZFCA	670	558	394	670	554	400	675	554	416
ZFEW	618	558	413	618	559	427	619	559	429
ZFTA	676	562	415	674	557	415	670	560	420
ZFGLy	669	552	398	675	560	418	-	560	392
ZFGLu	680	552	454	674	560	419	680	560	419
ZFU	700	559	413	680	557	420	700	557	424

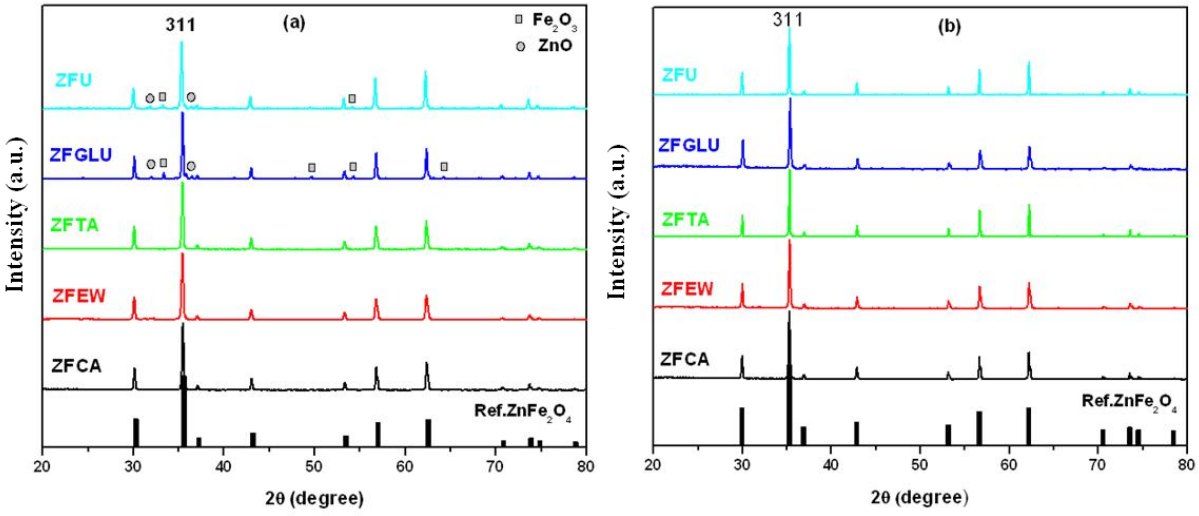

Figure 2. XRD patterns for ZF samples: (a) after heat treatment at 973 K (with Ref. $ZnFe_2O_4$, 82-1042, ICDD, JCPDS 2002), (b) after heat treatment at 1173 K (with Ref. $ZnFe_2O_4$, 89-1009 ICDD, JCPDS 2002).

exchange between the tetrahedral and octahedral spinel sites [7].

The FT-IR spectra in Figs. 1b-1d show for the samples heat treated at 773 K, 973 K and 1173 K, respectively, one main feature at near 550 cm^{-1}, attributable to v_1 and a feature at near 400 cm^{-1}, attributable to v_2. Fig. 1b shows the absence of the organic phase for all the samples, except the ZFEW sample which displays two peaks around 1100 cm^{-1} attributable to C-OH bond stretching vibrations and C-N bond stretching vibrations.

Table 2 summarizes the values of the vibrational modes v_1^*, v_1 and v_2 corresponding to ZF samples heat treated at 773 K, 973 K and 1173 K, respectively. The small variation of frequency value as a function of both fuel nature and heat treatment could be attributed simultaneously to the relationship between vibrational modes and crystallite size in the nanostructured materials [22] as well as to the redistribution of cations between interstitial sites which are responsible for changing of corresponding bond lengths [8].

3.2. XRD patterns interpretation

XRD patterns for the samples annealed at 973 K (Fig. 2a) and at 1173K (Fig. 2b), respectively, confirmed $ZnFe_2O_4$ spinel phase formation according to the typical indexed reflection plane (311). The influence of the combustion agent for single phase formation was observed. In the case of ZFAC, ZFAT, ZFEW and ZFGly, pure spinel phase was achieved after the thermal treatment at 973 K, while in the case of ZFU and ZFGLu samples, the secondary phases ZnO (hexagonal system, 80-0075, ICDD, JCPDS 2002) and Fe_2O_3 (rhombohedral system, 84-0311, ICDD, JCPDS 2002) were noticed (Fig. 2a). The presence of small amounts of the secondary phases (Table 3) only when using urea and glucose as fuels can be explained by a lower self-combustion temperature during synthesis

Table 3. XRD data for ZF samples heat treated at 973 K.

Sample	ZFCA	ZFEW	ZFTA	ZFGLy	ZFGLu	ZFU
Crystallite size (nm)	48	40	47	53	44	38
Lattice parameter (Å)	8.4183 ± 0.0101	8.4213 ± 0.0084	8.4186 ± 0.0103	8.4476 ± 0.0018	8.4139 ± 0.0088	8.4258 ± 0.0051
Secondary phases (%)					α–Fe_2O_3, 7.14±0.52 (%) ZnO, 4.60±0.41 (%)	α–Fe_2O_3, 6.32±0.44 (%) ZnO, 3.46±0.31 (%)
X-ray density (g cm^{-3})	5.3674	5.3616	5.3668	5.3117	5.3758	5.3530

which resulted in a possible segregation of ZnO and Fe_2O_3 phases within spinel lattice. Therefore, only for ZFU and ZFGLu samples, the pure spinel phase was accomplished after annealing at 1173 K (Fig. 2b).

Experimental and calculated data obtained from XRD patterns are given in Tables 3 and 4 for the samples heat treated at 973 K and at 1173 K, respectively. The average crystallite size for each sample in both annealing stages has been calculated from the half width value of the diffraction peak using Scherrer's equation [16]. Estimated error of determination was 2% of the calculated values. The smallest crystallite values were found for ZFU (38 nm) among samples heat treated at 973 K (Table 3), and for ZFGLu (51 nm) among samples heat treated at 1173 K (Table 4), respectively.

Zinc ferrite crystallizes in spinel-type cubic system belonging to $Fd\bar{3}4m$ space group, and the standard lattice parameter values range from 8.4125 Å (82-1042, ICDD, JCPDS 2002) to 8.4432Å (89-1009 ICDD, JCPDS 2002) which is in agreement with our experimental values (Tables 3 and 4).

The influence of the combustion agent is clearly noticeable when one considers gel forming duration, the level of sand bath's temperature at the ignition point and the post-ignition thermal treatment duration. These could be the primary causes of the cation arrangement in the spinel-type lattice, which affected the lattice parameter and bond length values. On the other side, the longer is the time of gel formation, the lower is the level of the sand bath temperature at the ignition point (Table 1) and by consequence the longer is the post-ignition thermal treatment duration. Therefore, the highest value of the experimental lattice parameter was obtained when using glycine as fuel with the most violent reaction mode at the lowest level of sand bath temperature.

According to previous studies, nanocrystalline zinc ferrite adopts a mixed spinel-type structure [23] for which the crystallographic formula is

$$\left(Zn^{2+}_{(1-x)}Fe^{3+}_{x}\right)\left[Zn^{2+}_{x}Fe^{3+}_{(2-x)}\right]O^{2-}_{4},$$

where *x* is the inversion degree that characterizes the Fe^{3+} ion concentration from the tetrahedral interstices (A), or the Zn^{2+} ion concentration from the octahedral interstices [B]. In order to confirm the experimental value of lattice parameter for ZFGLy sample, the existence of Fe^{2+} in B-site was proposed. This could be a consequence of Jahn-Teller effect [23]. The absence of the specific shoulder in the IR spectra could confirm the low Zn^{2+} concentration in the A-site at the expense of Fe^{3+} from B-site.

Using previous research as reference [24,25], Table 5 presents our proposed cation distribution and the computed lattice parameter values (estimated error, $\pm 10^{-5}$Å) for the pure spinel phases confirmed by XRD, bond lengths (R_A, R_B) and the oxygen positional parameter values u^{43m} for A-site and u^{3m} for B-site, respectively. The inversion degree and the lattice parameter values change with increasing heating temperature. This ocurrs as a consequence of the reverse transition of cations in the interstices towards their originating ideal arrangement of the normal spinel with the crystallographic formula.

3.3. SEM images interpretation

The influence of the combustion agent on the morphology and particle size of ZF powders synthesized by sol-gel auto-combustion method was evidenced from SEM micrographs of the annealed samples at 1173 K (Fig. 3).

All the ZF samples have the particle size in nanometer range. Fig. 3f shows for ZFU particles the coexistence of large cubic-shape particles with round corner and small spherical particles. The rest of ZF samples images reveal spherically shaped particles with a different degree of agglomeration. Voids and holes visible in Figs. 3a-3f are the effect of different amount of released gases during the combustion process as a

Table 4. XRD data, physical density and porosity for ZF samples heat treated at 1173 K.

Structural data for samples	ZFCA	ZFEW	ZFTA	ZFGLy	ZFGLu	ZFU
Crystallite size (nm)	60	57	62	61	51	55
Lattice parameter (Å)	8.4344 ± 0.0027	8.4382 ± 0.0011	8.4236 ± 0.0056	8.4422 ± 0.0007	8.4221 ± 0.0060	8.4332 ± 0.0035
X-ray density (g cm^{-3})	5.3367	5.3295	5.3572	5.3219	5.3560	5.3390
Physical density (g cm^{-3})	3.2797	3.4882	3.5999	3.1871	3.6163	3.4973
Porosity (%)	38.54%	34.54%	32.80%	40.11%	32.48%	34.49%

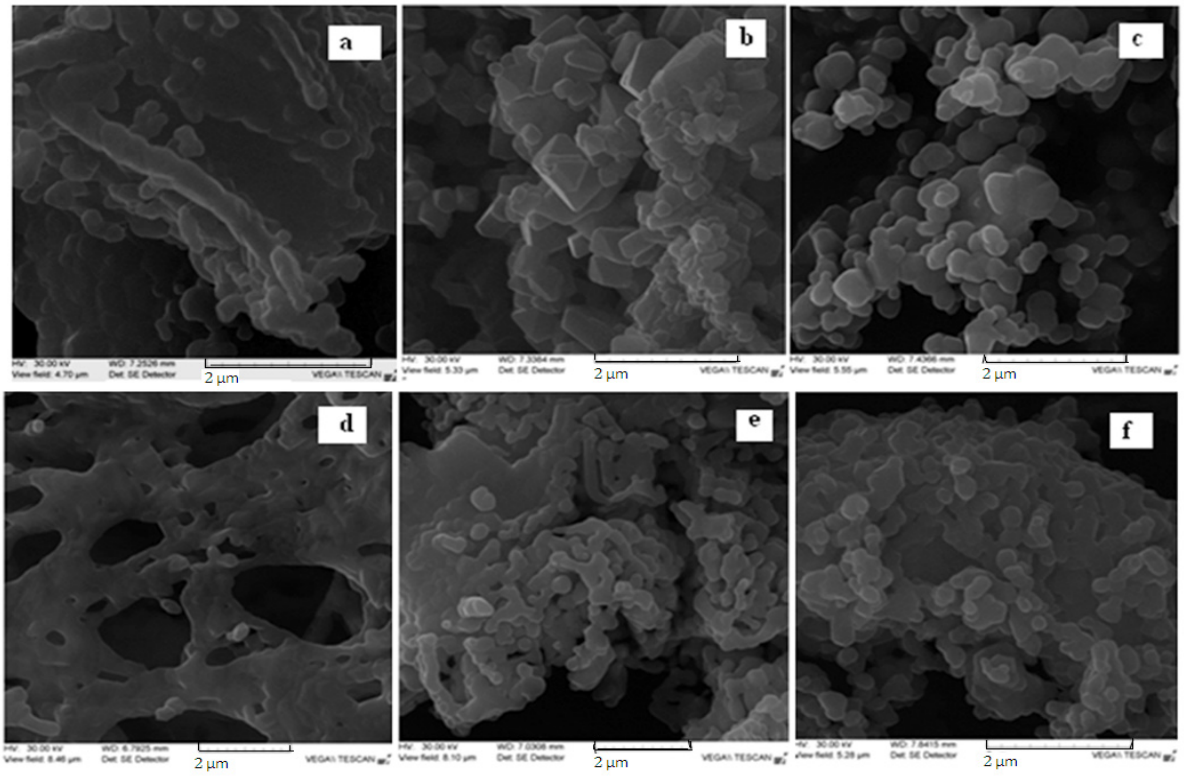

Figure 3. SEM micrographs for ZF samples after heat treatment at 1173 K: (a) ZFCA, (b) ZFEW (a) (c) ZFTA (d) ZFGLy (e) ZFGLu (f) ZFU.

function of fuel nature. The macroporosity is very high for ZFGLy powder due to the sponge-like microstructure (Fig. 3d). This feature is in good agreement with a previous study [26] and with our calculated value using XRD data (Table 4).

3.4. Magnetic properties interpretation

Fig. 4 presents magnetization curves measured at room temperature for powders annealed at 973 K and at 1173 K, respectively. The influence of the combustion agents and synthesis conditions on the magnetic behavior of the as-synthesized samples was observed. Our proposed cation distribution was confirmed by the magnetic measurements (Table 6). Based on the magnetization curves shape (Fig. 4-inset) and the specific magnetization values reached at maximum magnetic fields, the samples can be classified into two types of ferrite: paramagnetic (ZFAC, ZFEW, ZFAT) and weak ferrimagnetic (ZFGly, ZFGlu, ZFU). For the first type of nanopowders, the magnetization increases linearly with the applied magnetic field and does not saturate even at maximum value of the applied magnetic fields of 10 kOe. Ferrimagnetic samples have a magnetization curve characterized by very low values of specific magnetization and coercive fields. After the heat treatment at 1173 K, the two behaviors are preserved and some small differences appear only for the specific magnetization values.

Table 5. Theoretical lattice parameter (a_{th}), bond length (R_A and R_B), cation distribution, oxygen positional parameters (u) for single-phase ZF samples.

Sample	Heat treatment (K)	a_{th} (Å)	R_A (Å)	R_B (Å)	Cation distribution	$u^{\bar{4}3m}$ (Å)	$u^{\bar{3}m}$ (Å)
ZFCA	1173	8.4344	1.9439	2.0405	$(Zn^{2+}_{0.672}Fe^{3+}_{0.328})[Zn^{2+}_{0.328}Fe^{3+}_{1.672}]$	0.3831	0.2581
	973	8.4183	1.9025	2.0584	$(Zn^{2+}_{0.295}Fe^{3+}_{0.705})[Zn^{2+}_{0.705}Fe^{3+}_{1.295}]$	0.3805	0.2555
ZFEW	1173	8.4382	1.9537	2.0363	$(Zn^{2+}_{0.761}Fe^{3+}_{0.239})[Zn^{2+}_{0.239}Fe^{3+}_{1.761}]$	0.3837	0.2587
	973	8.4213	1.9102	2.0551	$(Zn^{2+}_{0.365}Fe^{3+}_{0.635})[Zn^{2+}_{0.635}Fe^{3+}_{1.365}]$	0.3810	0.2560
ZFTA	1173	8.4236	1.9145	2.0532	$(Zn^{2+}_{0.419}Fe^{3+}_{0.581})[Zn^{2+}_{0.581}Fe^{3+}_{1.419}]$	0.3813	0.2563
	973	8.4186	1.9032	2.0581	$(Zn^{2+}_{0.302}Fe^{3+}_{0.698})[Zn^{2+}_{0.698}Fe^{3+}_{1.302}]$	0.3805	0.2555
ZFGLy	1173	8.4421	1.8912	2.0739	$(Zn^{2+}_{0.193}Fe^{3+}_{0.807})[Zn^{2+}_{0.807}Fe^{2+}_{0.223}Fe^{3+}_{0.97}]$	0.3793	0.2543
	973	8.4475	1.9002	2.0707	$(Zn^{2+}_{0.275}Fe^{3+}_{0.725})[Zn^{2+}_{0.725}Fe^{2+}_{0.238}Fe^{3+}_{1.037}]$	0.3799	0.2549
ZFGLu	1173	8.4221	1.9122	2.0542	$(Zn^{2+}_{0.384}Fe^{3+}_{0.616})[Zn^{2+}_{0.616}Fe^{3+}_{1.384}]$	0.3811	0.2561
ZFU	1173	8.4332	1.9408	2.0419	$(Zn^{2+}_{0.644}Fe^{3+}_{0.356})[Zn^{2+}_{0.356}Fe^{3+}_{1.644}]$	0.3829	0.2579

The magnetic properties of the as-synthesized ferrites are strongly dependent on the fuel agent, as they develop different temperature at an ignition moment which, in result, promotes differences in cation placements within interstices when spinel phase is forming. According to Zaki *et al*. [23] and Hankare *et al*. [27], there is a correlation between IR spectra study, inversion degree and magnetic behavior of ferrites. We performed a similar analysis for our samples.

Table 6 presents the same trend for ZF samples annealed at 1173K in terms of inversion degree, bond length gradient for both sites (R_B-R_A), wavenumber gradient (v_1-v_2), half bandwidth (HBW) of v_1 and specific magnetization values (M). The calculated value of HBW of v_1 could be indicative of Zn^{2+}/Fe^{3+} substitution from tetrahedral site [23]. This is in accordance with the proposed cation distribution presented in Table 5.

The more trivalent cations of Fe^{3+} are located in A site, the highest is A-B magnetic interaction. Therefore, we found the highest M value for ZFGLu and ZFGLy samples which have the highest values for the inversion degree. At the same time, an increase of the wavenumber gradient is affected by the corresponding increase of bond lengths gradient. In terms of unit cell symmetry, an increase of bond lengths gradient leads to a decrease of the distance between A and B sites. This could be responsible for the increase of A-B super-exchange interaction, thus affecting the magnetic behavior [27].

Table 6 shows a good correlation between structural results, the proposed cation distribution and the experimental value of specific magnetization.

4. Conclusions

In the present work, a interrelationship among sol-gel auto-combustion synthesis conditions, structure and magnetic properties of zinc ferrite nanoparticles were reported

The nature of the fuel affects the auto-combustion reaction intensity and the duration of thermal treatment, which dictates specific structural characteristics and magnetic properties of the samples.

From IR spectra of the zinc ferrite samples, the appearance of the vibrational modes specific to metal-oxygen bonds of both tetrahedral and octahedral sites was observed. Small differences of the vibrational mode values were noticed between samples as a consequence of fuel agent. The values of bond length gradient for both sites, wavenumber gradient and half bandwidth were studied in connection with inversion degree and specific magnetization values of the as-obtained samples.

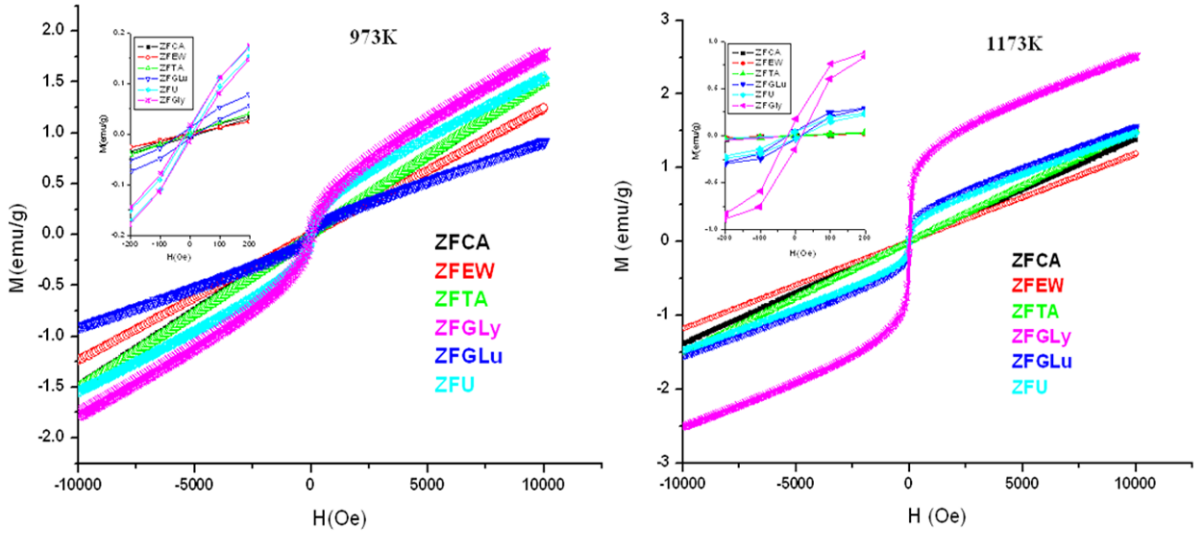

Figure 4. Magnetization vs. applied magnetic field for ZF samples at room temperature: after heat treatment at 973 K (left) and after heat treatment at 1173 K (right).

Table 6. Comparative trend between inversion degree value, FT-IR and VSM data.

Sample	x (inversion degree)	R_B-R_A(Å)	v_1- v_2(cm^{-1})	HBW(cm^{-1})	M (emu g^{-1})
ZFEW	0.239	0.0826	130	64	1.19
ZFCA	0.328	0.0966	138	72	1.4
ZFU	0.356	0.1011	133	74	1.48
ZFTA	0.581	0.1387	140	77	1.51
ZFGLu	0.616	0.1420	141	90	1.55
ZFGLy	0.801	0.1827	168	85	2.51

From X-ray patterns, a monophase spinel type formation was confirmed, and values of crystallite size, parameter value and X-ray density were evaluated comparatively. Value of the inversion degree was calculated for the samples annealed at 973 K and 1173 K and studied as a function of fuel nature.

From SEM images, it was observed that the nature of the fuel influenced the shape of particles, agglomeration degree and texture of zinc ferrite samples.

Citric acid, tartaric acid, glycine and egg white could be considered good candidates for obtaining monophase Zn ferrite nanoparticles at low level of calcination temperature (973 K) using sol-gel auto-combustion method.

In order to obtain small nanocrystallite (≈ 50 nm) size for zinc ferrite with ferrimagnetic behavior, glucose or glycine could be a successful fuel choice. Small nanocrystallite size (≈ 40 nm) of zinc ferrite with paramagnetic behavior could be obtained by using egg white as fuel.

Comparison our results with those reported in the literature may conclude that in the case of Zn ferrite powders, the nature of fuel agent and combustion synthesis conditions have a significant influence on the vibrational mode values, crystallite size, lattice parameter, inversion degree value, morphology and the spin disorder at the nanoparticles surface, implicitly on the specific magnetization value.

Through this study we revealed the importance of fuel agent and synthesis conditions on structural features and magnetic properties of zinc ferrite nanoparticles with dual functionality and with potential applications for targeted and triggered drug release, image guided therapy including validation of delivery and therapy response.

Acknowledgment

The authors Tamara Slatineanu and Valentin Nica thank for the financial support from the European Social Fund in Romania, under the responsibility of the Managing Authority for the Sectoral Operational Programme for Human Resources Development 2007-2013 [grant POSDRU/88/1.5/S/47646] and [grant POSDRU/89/1.5/S/49944], respectively.

References

[1] N. Kikukawa, M. Takemori, Y. Nagano, M. Sugasawa, S. Kobayashi, J. Magn. Magn. Mater. 284, 206 (2004)
[2] C. Barcena, A.K. Sra, Girija S. Chaubey, C. Khemtong, J. Ping Liub, J. Gao, Chem. Commun. 2224 (2008)
[3] X. Niu,W. Du and W. Du, Sens. Actuators B: Chemical 99, 405 (2004)
[4] H. Lee, J.C. Jung, H. Kim, Y.-M. Chung, T.J. Kim, S.J. Lee, S.-H. Oh, Y.S. Kim, I.K. Song, Catal. Commun. 9, 1137 (2008)
[5] H. Ehrhardt, S.J. Campbell, M. Hofmann, Scripta Mater. 48, 114 (2003)
[6] T. Shimada, T. Tachibana, T. Nakagawa, T.A. Yamamoto, J. Alloys Compd. 379, 122 (2004)
[7] G. Fan, Z. Gu, L. Yang, F. Li, Chem. Eng. J. 155, 534 (2009)
[8] A. Pradeep, P. Priyadharsini, G. Chandrasekaran, J. Alloys Compd. 509, 3917 (2011)
[9] H. Xue, Z. Li, X. Wang, X. Fu, Mater. Lett. 61, 347 (2007)
[10] C. Yao, Q. Zeng, G.F. Goya,T. Torres, J. Liu, H. Wu, M. Ge, Y. Zeng, Y. Wang, J.Z. Jiang, J. Phys.Chem. C 111, 12274 (2007)
[11] M. Sivakumar, T. Takami, H. Ikuta, A. Towata, K. Yasui, T. Tuziuti, T. Kozuka, D. Bhattacharya, Y. Lida, J. Phys. Chem. B 110, 15234 (2009)
[12] C. Upadhyay, H.C. Verma, V. Sathe, A.V. Pimpale, J. Magn. Magn. Mater. 312, 271 (2007)
[13] M. Mozaffari, M. Eghbali Arani, J. Amighian, J. Magn. Magn. Mater. 322, 3240 (2010)
[14] P. Hu, D. Pan, X. Wang, J. Tian, J. Wang, S. Zhang, A. A. Volinsky, J. Magn. Magn. Mater. 323, 569 (2011)
[15] P. Laokul, V. Amornkitbamrung, S. Seraphin, S. Maensiri, Current Appl. Phys. 11, 101 (2011)
[16] T. Slatineanu, A.R. Iordan, M.N. Palamaru, O.F. Caltun, V. Gafton, L. Leontie, Mater. Res. Bull. 46, 1455 (2011)
[17] C.-C. Hwang, T.-Y. Wu, J. Wan, J.-S. Tsai, Mater. Sci. Eng. B 111, 49 (2004)
[18] S. Maensiri, C. Masingboon, B. Boonchom, S. Seraphin, Scripta Mater. 56, 797 (2007)
[19] H.P. Klug, L.E. Alexander, X-ray diffraction procedures for polycrystalline and amorphous materials (Wiley, New York, U.S.,1974)
[20] S.S. Bathu, V.K. Lakhani, A.R. Tanna, N.H. Vasoya, J.H. Buch, P.U. Sharma, U.N. Trivedi, H.H. Joshi, K.B. Modi, Indian J. Pure&Appl. Phys. 45, 596 (2007)
[21] R.D. Waldron, Phys. Rev. 99, 1727 (1955)
[22] M. Thomas, K.C. George, Indian J. Pure & Appl. Phys. 47, 81 (2009)
[23] H.M. Zaki, H.A. Dawoud, Phys. B 405, 4476 (2010)
[24] R.D. Shannon, Acta Cryst. A32, 751 (1976)
[25] K.E. Sickafus, J.M. Wills, J. Am. Ceram. Soc. 82, 3279 (1999)
[26] A.C.F. M. Costa, V.J. Silva, C.C. Xin, D.A. Vieira, D.R. Cornejo, R.H.G.A. Kiminami, J. Alloys Compd. 495, 503 (2010)
[27] P.P. Hankare, R.P. Patil, U.B. Sankpal, S.D. Jadhav, K.M. Garadkar, S.N. Achary, J. Alloys Compd. 509, 276 (2011)